Multimodal characterization of acid-pretreated poplar reveals spectral and structural parameters strongly correlate with saccharification

Aya Zoghlami, Yassin Refahi, Christine Terryn, Gabriel Paës

Multimodal characterization of acid-pretreated poplar reveals spectral and structural parameters strongly correlate with saccharification

Aya ZOGHLAMI[1], Yassin REFAHI[1], Christine TERRYN[2], Gabriel PAËS[1*]

[1] FARE Laboratory, INRA, Université de Reims Champagne Ardenne, Reims, France

[2] Platform of Cellular and Tissular Imaging (PICT), Université de Reims Champagne Ardenne, Reims, France.

*Author for correspondence: Gabriel Paës, gabriel.paes@inra.fr

Highlights:

- Multiscale characterization of dilute acid pretreated poplar samples was performed
- A severity threshold effect (2.5-2.7) affecting lignin organization is identified.
- Hydrolysis can be predicted by autofluorescence and Raman spectroscopy
- Cellular sphericity is negatively correlated with hydrolysis yield
- Quantitative relations across scales highlight recalcitrance

Abstract

Lignocellulose biomass can be transformed into sustainable chemicals, materials and energy but its natural recalcitrance requires the use of pretreatment to enhance subsequent catalytic steps. Dilute acid pretreatment is one of the most common and efficient ones, however its impact has not yet been investigated simultaneously at nano- and cellular-scales. Poplar samples have been pretreated by dilute acid at different controlled severities, then characterized by combined structural and spectral techniques (scanning electron microscopy, confocal microscopy, autofluorescence, fluorescence lifetime, Raman). Results show that pretreatment favours lignin depolymerization until severity of 2.4-2.5

while at severity of 2.7 lignin seems to repolymerize as revealed by broadening of autofluorescence spectrum and strong decrease in fluorescence lifetime. Importantly, both nano-scale and cellular-scale markers can predict hydrolysis yield of pretreated samples, highlighting some connections in the multiscale recalcitrance of lignocellulose.

Keywords: Lignocellulose, Recalcitrance, Multiscale, Pretreatment, Hydrolysis

1. Introduction

The environmental effects of climate change and fast depletion of fossil resources (Trends, 2017) have promoted the development of alternative energy sources and bio-based chemicals and polymers. Lignocellulosic biomass (LB) is an important feedstock to produce such sustainable products and can be a solution to increasing concerns over energy demand and climate change without compromising global food security (Yuan et al., 2018).

LB is mainly composed of cellulose and hemicelluloses which are carbohydrate polymers and of lignin which is a highly branched phenylpropanoid polymer. The different biomass feedstocks (mainly wood and grass biomass species) have significant differences in proportion of the main constituents (Zhao et al., 2012a). While cellulose and lignin are more abundant in woody biomass, grass biomass has higher proportion in hemicelluloses. LB includes dedicated energy crops growing on low-quality soil such as miscanthus or switchgrass. Also considered as LB resources are agricultural wastes such as cereal straw, bagasse and forest biomass such as forest and mill residues and woody crops such as poplar and pine.

Main issue in the transformation of LB is that it is naturally recalcitrant to deconstruction into bio-based products because of its complex structure and chemical composition (Zhao

et al., 2012b). Several factors underlying LB recalcitrance have been identified such as the content of lignin/hemicellulose/cellulose (Studer et al., 2011), cellulose crystallinity (Xu et al., 2019), the degree of cellulose polymerization (Hallac & Ragauskas, 2011) and pore size/density (Meng et al., 2015)To overcome the recalcitrance of lignocellulose, a pretreatment step is essential to facilitate LB enzymatic hydrolysis. The pretreatment changes the physical and/or chemical structure of LB and facilitates the conversion of polysaccharides into fermentable sugars by enzymes by increasing accessibility to enzymes (McCann & Carpita, 2015). A wide range of pretreatment methods have been developed which can be classified into physical (e.g. milling, irradiation (e.g. Gamma-ray)), chemical & physico-chemical methods (e.g. explosion (with steam), acid (sulfuric)), and biological (fungi and actinomycetes) methods. Pretreatment is an expensive step in LB conversion process and the choice of the pretreatment type depends on the biomass species, due to variations in the content and composition of lignin and hemicellulose among LB species.

Dilute Acid Pretreatment (DAP) is one of the most commonly used industrial methods of pretreatment due to its relatively low cost and its efficiency particularly with hardwoods (Silveira et al., 2015). The DAP is mostly performed using 0.4-2.0% (w/w) H_2SO_4 at a temperature of 160-220°C (Cao et al., 2012). It solubilizes hemicelluloses, disrupts the lignin structure, and increases cellulose accessibility to enzymes (Santos et al., 2018) favoring subsequent enzymatic hydrolysis. The influence and efficiency of the DAP depends on the pretreatment temperature, acidity (pH) and residence time. An indication of pretreatment harshness can be represented by a single value called CSF (Combined Severity Factor) (Lee & Jeffries, 2011). Despite extensive studies investigating the influence of the DAP on LB physico-chemical structure and morphology, the effect of the DAP at cellular and tissular scale remains yet poorly explored.

In this article, we have selected poplar (*Populus nigra* x *deltoides*) as a model of hardwood to investigate the effect of DAP pretreatment on LB at multiple scales under different pretreatment severities. Indeed, poplar is the first woody plant to have its genome sequenced (Chang et al., 2016), it has a fast growth rate, an easy in vitro cultivation and vegetative propagation as well as extensive geographical distribution (Meng et al., 2017). Moreover, the possibility of performing genetic modifications in poplar turns it into one of the most promising species for reducing LB recalcitrance (Lee & Jeffries, 2011). In order to investigate the effect of DAP pretreatment on poplar, compositional, structural and topochemical changes of poplar samples during DAP and cellulose digestibility were measured. This multimodal analysis was carried out using different microscopy techniques including advanced fluorescence microscopy techniques, chemical composition analysis by confocal Raman microscopy, scanning electron microscopy, and enzymatic hydrolysis to monitor the changes of substrate properties. Correlation between chemical / structural information and digestibility was finally done to highlight the impacts of specific markers on recalcitrance.

2. Material and methods

2.1 Sample preparation

Poplars (*Poplus nigra* x *deltoides*) of about 2 years old were collected in Estrées-Mons, France. The collected poplar dried stems were cut into fragments of 0.4 cm wide, 2 cm long, 0.2 cm thickness using a razor blade. Poplar fragments were pretreated in a batch mode using mineralization bombs equipped with Teflon cups. 500 mg of poplar samples were presoaked in 2% (v/v) sulfuric acid (solution at a ratio of 1:30) and incubated in an oil bath at 170°C for 10, 15 and 20 minutes corresponding to three combined severity factor (CSF) of 2.4, 2.5 and 2.7, respectively. **These conditions were chosen because a**

lower temperature did not provide significant modifications of the tissue architecture while higher temperature strongly damaged the tissues so that microscopy analysis was no longer possible. The CSF integrates the reaction time, temperature and acid concentration into a single value and represents the pretreatment harshness. The CSF is computed using the formula CSF = $\log_{10}(t.\exp[(T_H-T_R)/14.75] - pH)$ as previously defined (Chum et al., 1990), where t is the reaction time in minutes, T_H is the temperature in °C, T_R is a reference temperature (typically 100°C) and pH is the acidity of the aqueous solution. Following DAP pretreatment of the samples, the Teflon cups were immersed in an ice bath for 5 min. The pretreated fragments were then washed three times with a 50% ethanol solution and three times with deionized water until the pH of the wash reached 7.0 to stop the acid hydrolysis. The samples were dried for 24 hrs at room temperature. To acquire microscopy images, the dried fragments were sectioned in the transverse plane from the xylem using a sliding microtome 40µm thickness. **All sections used for microscopic analysis were made 0.5 cm thickness starting from the edge to be sure to have a homogeneous effect of the pretreatment.**

To perform chemical composition analysis and enzymatic saccharification, the dried samples were milled into particles with 80 µm diameter (granulometry measurement). Untreated fragments were cut using a sliding microtome into sections of 40 µm thickness or milled into 80 µm diameter particles for imaging, chemical composition and enzymatic saccharification analysis.

2.2 Chemical composition and enzymatic saccharification

The chemical composition including moisture, ash, lignin, and carbohydrates' contents of untreated and pretreated poplar samples was determined using the methods already described (Herbaut et al., 2018). The enzymatic hydrolysis assays were performed on both

126 untreated and pretreated samples using a commercial cellulase preparation Cellic ® CTec2
127 (Novozymes A/S Bagsværd, Danemark), selected for its hydrolysis efficiency with a
128 cellulase activity of 195 FPU/mL measured by the filter paper method. Enzymatic
129 saccharification of poplar samples (2 % w/v) was carried out in 10 mL acetate buffer
130 (0.05M, pH 5) for 72 hrs at 50°C and 200 rpm containing 0.02 % sodium azide and the
131 Cellic ® CTec2 cocktail with a final enzyme concentration of 20 FPU/g of dry matter.
132 The reaction mixtures (buffer and sodium azide) were pre-incubated for 30 min at 50°C
133 and 200 rpm. The enzymatic hydrolysis was then initiated by adding the enzymatic
134 cocktail. During the enzymatic hydrolysis, the samples were kept at 50°C for 72 hrs.
135 Aliquots were taken at different timepoints: 0, 0.5, 1, 2, 4, 6, 8, 24, 32, 56 and 72 hrs to
136 compute hydrolysis kinetics (Auxenfans et al., 2017a). The concentration of glucose
137 released from enzymatic hydrolysis in the supernatant was determined using a high-
138 performance anionic exchange chromatography (HPAEC-PAD, Dionex) to calculate the
139 cellulose conversion from the untreated and pretreated poplar, as follows:
140 Cellulose conversion (%)
141 = Amount of released glucose/Amount of cellulose in samples before hydrolysis x 100
142 All experiments and analysis were carried out three times (biological triplicate).
143

144 **2.3 Scanning electron microscopy (SEM)**

145 To investigate and compare the surface morphology changes between untreated and
146 pretreated samples, the samples were observed using a binocular microscope (Stemi 2000-
147 C, Zeiss,Germany), then imaged by scanning electron microscopy (SEM) using an
148 environmental tabletop electron microscope Hitachi TM-1000 (Japan) in low-vacuum
149 mode. SEM pictures of untreated and pretreated poplar sections were acquired at, 600x and
150 3000x magnifications.

151

152 **2.4 Confocal Raman microscopy (CRM)**

153 The untreated and pretreated poplar sections were pre-incubated in water for 30 min and
154 then placed on a quartz slide with a drop of ultrapure water and sealed with a cover slip
155 (0.17 mm thickness) to avoid evaporation during the Raman signal detection. Raman
156 spectra were acquired with a microspectrometer LabRam ARAMIS (Horiba Jobin-Yvon,
157 Villeneuve d'Ascq, France). The laser source was a diode at 785 nm to avoid fluorescence
158 (Zeng et al., 2016), with 13mW power on sample. The microspectrometer was coupled to a
159 microscope BX41 (Olympus, France) equipped with a motorized (x, y) stage. All
160 measurements were recorded using a 100x water immersion objective (LUMPlanFI, NA =
161 1.0, Olympus, France). The laser and the light scattered by sample were collected through
162 the same objective. A confocal pinhole rejects signals from out-of-focus regions of the
163 sample. A multichannel charge-coupled-channel device (1024x256 pixels) was used to
164 detect the Raman Stokes signal dispersed by a holographic grating (1200 lines/mm)
165 (Gierlinger et al., 2012; Chen et al., 2016a). Raman spectra were recorded with LabSpec 5
166 software (Horiba, Jobin Yvon, Villeneuve d'Ascq, France) in the specific spectral range
167 950-1700 cm^{-1}. Three samples for each condition of pretreatment were analysed and for
168 each sample ten spectra were recorded on different regions of cell wall (cell corner (CC),
169 compound middle lamella (CML) and secondary wall (SW)). These spectra were averaged
170 for each sample. Then, a pre-treatment of Raman spectra was performed with a homemade
171 interface in Matlab were smoothed using Savitzky-Golay function (5 points, 3^{rd}
172 polynomial order) and baseline corrected (3^{rd} polynomial order). Bands were assigned
173 according to the literature are summarized in Table 1.

174

175 **2.5 Laser Scanning Confocal Microscopy for 3D imaging**

2.5.1 3D image acquisition

Poplar cross sections were incubated in 0.05 M acetate buffer at pH 5 for 30 min prior to mounting in the same medium on a microscope slide and covered with a cover slip (0.17 mm thickness). Using a confocal laser scanning microscope (Leica TCS SP8, Germany) equipped with 63× oil-immersion objective (NA = 1.4), z-stacks (0.3µm) of both untreated and pretreated poplar samples were acquired at scan speed of 400 Hz. A 405 nm laser (4% intensity) was used for imaging cell wall sample autofluorescence by detecting fluorescence emission on the 415-700 nm range using the HyD detector in counting mode. The z-stacks were acquired with a resolution of 512 x 512 pixels. The microscope parameters and image resolution were optimized to avoid sample photo-bleaching.
For each pretreatment condition (CSF = 2.4, 2.5, 2.7) as well as untreated samples, z-stacks on three different randomly selected areas of three different samples were acquired.

2.5.2 Image analysis and 3D segmentation of confocal images

Acquired z-stacks were processed using an automated 3D segmentation and quantification pipeline. The original z-stacks were then saved in tif files with customized tags which guaranteed that the metadata (e.g. voxel dimensions, file type) were saved properly. The images were then denoised using Alternating Sequential Filter (ASF) and Gaussian filters (Willis et al., 2016; Michelin et al., 2016). To segment the filtered z-stack in order to identify individual cell walls, the z-stack was first segmented using a 3D watershed algorithm whose seeds were determined using the h-minima operator which computed local minima regions in the denoised z-stacks. The 3D watershed algorithm provided a 3D image in which voxels (volumetric pixel) of the same cell were labeled by a unique integer as cell identifier. Thresholding was then used to compute cell walls by replacing the voxels of the segmented images with background value (fixed to 1) if the intensity of the

corresponding voxels on filtered z-stack was below a global threshold. The segmentations were visually inspected for segmentation error (over-segmentation, under-segmentation, missed cell, or shape error) and the segmentation parameters were subsequently optimized (Willis et al., 2016).

2.5.3 Quantification of cellular scale structural parameters

Following 3D segmentation of z-stacks, individual cell wall volumes were computed by counting the number of voxels which had the same label and multiplying this number by the voxel volume which was approximately $0.039\mu m^3$. Cell wall surface area was estimated from triangular meshes of cell wall surfaces obtained using the marching cubes algorithm from the Visualization Toolkit (VTK) (Willis et al., 2016; Schroeder et al., 2004). Then volume, V, and surface area, A, were computed to determine sphericity $\Psi = \frac{6\pi^{1/3}V^{2/3}}{A}$, a dimensionless cellular scale parameter, for each individual cell.

2.6 Laser Scanning Confocal Microscopy for spectral imaging

2.6.1 Autofluorescence

Spectral images of untreated and pretreated poplar samples were acquired using laser scanning microscope LSM 710 NLO Zeiss (Zeiss SAS, Germany) coupled with a Chameleon TiSa accordable 80 MHz pulsed laser (COHERENT, USA). Samples sections (40 µm) were mounted in 0.5 M acetate buffer at pH 7 and their excitation was performed using a biphoton excitation at 750 nm. Spectral images were acquired using spectral detector (32 channel simultaneously) of the microscope between 420 and 722 nm using a 20x objective (NA = 0.8). Fluorescence images of untreated and pretreated samples were colored based on their spectrum (each of the 32 channels was represented by its corresponding color from blue to red).

226

227 **2.6.2 Fluorescence lifetime measurement and analysis**

228 The fluorescence lifetime imaging (FLIM) measurements were performed on untreated
229 and pretreated poplar sections between 455 and 655 nm using a spectral time-correlated
230 single photon counting (TCSPC) detector from Becker and Hickl (Becker & Hickl, Berlin,
231 Germany). Data were analyzed using a multi-exponential decay model with 2 components
232 using SPCImage software (Becker & Hickl, Berlin, Germany). Measurement of average
233 fluorescence lifetime was made by applying regions of interest (ROIs) to cell wall regions
234 such as cell corner (CC), compound middle lamella (CML) and secondary wall (SW) for
235 untreated and pretreated poplar using 10 replicate measurements on each of the 3 regions.
236 ROI data were summed to provide estimates of distributions in these regions.

237

238 **2.7 Data and statistical analysis**

239 All the experiments were carried out in triplicate, and the results were expressed as means
240 ± standard deviations. Analysis of variance (ANOVA) was performed on the obtained data
241 followed by a Tukey's post hoc test for comparison between the untreated and pretreated
242 poplar. *p*-value for statistical difference was set to 0.05. Statistical analyses were
243 performed using the SigmaPlot 12.0 software (Systat Software, Chicago, USA). Kruskal-
244 Wallis test from SciPy library was performed on computed cellular sphericity values from
245 untreated and pretreated datasets.

246

247 **3. Results and Discussion**

248 **3.1 DAP changes LB chemical composition and improves enzymatic saccharification**

249 The chemical composition of biomass samples is a significant factor that affects the
250 sequential enzymatic hydrolysis. In order to better understand the changes induced by the

different degree of severity of the DAP, the chemical composition of both untreated and pretreated samples was analysed. Cellulose, hemicelluloses, lignin, moisture and ash content were determined on a dry weight basis (Fig. 1). The untreated poplar contained ca. 40% ± 0.4 cellulose, 21% ± 0.2 hemicelluloses with xylose as the major component (also comprising arabinose, rhamnose, mannose and uronic acids) and 26% lignin, which is consistent with reports from the literature (Herbaut et al., 2018; Esteghlalian et al., 1997). As expected, hemicelluloses solubilisation increased significantly with pretreatment severity. About 70% of the hemicellulose fraction was removed from the pretreated substrate under the most severe pretreatment conditions (CSF 2.7). The decrease in hemicellulose content, proportional to the pretreatment severity, was due to its degradation into other chemicals under higher temperature and acid conditions. The lignin content gradually increased with increasing CSF: this result is due to the concomitant loss of hemicellulose and the formation of condensed lignin products (Sannigrahi et al., 2011). This could also be due to the formation of pseudo-lignin by the combination of carbohydrates and lignin degradation products (Sannigrahi et al., 2011). Many studies reported similar changes in carbohydrates and lignin content after DAP (Herbaut et al., 2018; Chen et al., 2016b).

In order to evaluate the efficiency of DAP on cellulose digestibility, the same samples used for the chemical composition analysis were subjected to a 72 hrs enzymatic hydrolysis using commercial cellulase cocktail Cellic CTec 2 with a loading of 20 FPU/g of dry matter. The effect of the different severity of DAP on poplar digestibility was estimated by determining the percentage of cellulose conversion over 72 hrs (Fig. 2). A remarkable increase in the efficiency of cellulose conversion was observed when DAP severity was increased, which confirms that pretreatment reaction time is a factor affecting the effectiveness of pretreatment (An et al., 2019). Indeed, the cellulose conversion of

276 untreated poplar was about 11% ± 0.11 after 72 hrs, then reached 17% ± 0.41 for
277 pretreated poplar at CSF 2.4, 28% ±0.77 (more than 2-fold) for pretreated poplar at CSF
278 2.5 and 58% ± 2.17 (5-fold) for pretreated poplar at CSF 2.7, which is in agreement with
279 results reported in the literature (Meng et al., 2016; Linde et al., 2008; Chen et al., 2018).
280 Overall, results confirm that DAP increases the efficiency of enzymes by improving their
281 accessibility, likely due to hemicellulose removal and lignin reorganization.
282
283 **3.2 SEM images reveal effect of DAP on cellular morphology**
284 To better understand the significant enhancement of poplar samples enzymatic digestibility
285 after pretreatment, the morphology of the untreated and pretreated samples was
286 investigated by SEM. Initially, the most apparent effect of the DAP observed by binocular
287 microscope was the color change of samples from yellow to dark brown which was more
288 pronounced in samples pretreated at high severity . Previous studies have reported that this
289 color change originated from chemical degradation of carbohydrates, lignin and wood
290 extractives (Negro et al., 2003). The cell walls of untreated poplar observed by SEM had a
291 rigid and highly ordered structure. The compound middle lamella (CML) and the
292 secondary wall (S2) kept close together. This rigid structure is recognized as a structural
293 organization limiting the accessibility of enzymes to cellulose (Mansfield et al., 1999). The
294 pretreated samples showed fiber deformation especially for the pretreated samples at CSF
295 2.5 and CSF 2.7. Poplar samples pretreated at the highest severity even showed fiber
296 separation (loss of the fibrous network) and formation of cracks emphasized by the
297 detachment between CML and S2. This structural change could be related to the
298 solubilisation of the hemicellulose fraction which is considered as the adhesive between
299 cell wall sublayers (Ling et al., 2015).
300

3.3 Raman microscopy shows DAP induced topochemical modifications

Confocal Raman microscopy provides information about the concentration and the spatial distribution of chemical components in cell walls (Gierlinger & Schwanninger, 2006). In this study, changes in the spatial distribution of polymers in the cell walls of pretreated poplar were investigated in situ. The average Raman spectra of untreated and pretreated poplar were collected from various regions: cell corner (CC), compound middle lamella (CML), and secondary wall (SW).

The spectral range from 950 to 1700 cm^{-1} includes bands from the wood components such as cellulose, hemicelluloses and lignin. Band assignment for poplar is shown in Table 1. Typical bands of lignin are in the region between 1500 cm^{-1} and 1700 cm^{-1} with specific peaks at 1604 cm^{-1} and 1660 cm^{-1}. The bands at 1036 cm^{-1}, 1095 cm^{-1} and 1123 cm^{-1} are attributed to carbohydrates.

For untreated poplar, the spectra from different cell wall regions presented different features. Lignin bands at 1604 cm^{-1}, 1275 cm^{-1} and 1331 cm^{-1} were higher in the spectra of CC and CML than those in SW, which in accordance with the higher content in lignin of CC. Contrary, the peaks at 1095 cm^{-1}, 1123 cm^{-1} and 1150 cm^{-1} were more pronounced in the SW than in CC and CML, indicating that SW mainly contains polysaccharides. Previous studies reported similar results (Chen et al., 2016a; Chen et al., 2018; Gierlinger & Schwanninger, 2006).

DAP caused considerable changes in the band intensity for the majority of Raman peaks, also depending on cell wall regions. The intensity of the band at 1604 cm^{-1}, which is related to lignin, increased significantly for CC and CML after DAP especially for the pretreated samples at CSF 2.5 and CSF 2.7 . It can be explained by the fact that lignin was more exposed after the removal of hemicelluloses during the DAP. It may also result from the dissolved lignin redeposited onto cell wall surfaces upon cooling after DAP. The

increase of the lignin band intensity for the SW was less important which can be explained by the low lignin content in this region. The peak at 1660 cm^{-1}, which is indicative of coniferyl alcohol and aldehyde (lignin-CAA) (Ma et al., 2013), has completely disappeared from Raman spectra of pretreated poplar at CSF 2.5 and CSF 2.7 particularly in the CC and CML. One possible explanation is that high severity DAP removes lignin-CAA structures. Previously, it has been reported that lignin is cross-linked with hemicelluloses that embed cellulose fibres and lignin-CAA associates with hydroxyl groups of cellulose and hemicelluloses via hydrogen bonding within cell walls. The removal of hemicelluloses during DAP may disrupt the cross-linked structures. This observation is consistent with the results from a study of the impact of alkali pretreatment on poplar cell walls (Ji et al., 2014). However, a significant decrease in the bands at 992 cm^{-1} , 1095 cm^{-1} and 1123 cm^{-1} was noted, more important in the SW than that in the CML and CC, indicating significant removal of the polysaccharides from the SW region after DAP and correlated with DAP severity. This topochemical analysis reveals that modifications in chemical composition after DAP are heterogeneous throughout the poplar cell walls and stronger with higher DAP severity.

3.4 DAP impacts cell wall autofluorescence and fluorescence lifetime

In wood, lignin is the predominant fluorophore exhibiting autofluorescence under UV light excitation (Donaldson & Radotic, 2013). Fig. 3A-D shows the autofluorescence of untreated and DAP poplar samples. While the spectral confocal image of untreated poplar (Fig. 3A) has a homogenous blue color distribution along the cell wall, this color turns to blue-greenish for pretreated poplar with CSF 2.5 (Fig. 3C) and to green-yellowish for pretreated poplar with CSF 2.7 (Fig. 3D). Changes in autofluorescence are likely to reflect modification of the lignin chemistry during DAP. Indeed, several factors related to lignin

are recognized as influencing fluorescence, such as content in lignin and in carbonyl groups, lignin condensation and cross-linkages between lignin and other cell wall components (Auxenfans et al., 2017b). Spectral data were analysed for all the untreated and DAP samples in different cell wall regions like for Raman measurements. The untreated poplar has a narrow emission band centred on the blue spectral range (maximum 478 nm) (Fig. 3E), with the CC and CMC spectra being close to each other and higher than SW spectrum. With the increase of DAP severity, the emission maximum expands in the green and yellow range (Fig. 3F-H) together with an increase in the fluorescence intensity and a distinct separation of the spectra corresponding to the cell wall regions. This result suggests that the DAP changed strongly the natural lignin arrangement, by solubilizing lignin molecules that interact with hemicellulose oligomers to form new fluorescent compounds emitting in the blue, green and yellow spectra. These results are in agreement with those previously published (Coletta et al., 2013; Li et al., 2007) and show how autofluorescence can reveal changes in lignin composition and arrangement after pretreatment.

Fluorophore lifetime is the average time between excitation of a fluorophore and emission of a fluorescence photon. Accordingly, fluorescence lifetime imaging microscopy (FLIM) is a technique to determine the spatial distribution of excited state lifetimes in microscopic samples (Van Munster & Gadella, 2005). In complement to autofluorescence, FLIM can advantageously be related to chemical properties of lignin (Auxenfans et al., 2017b ; Chabbert et al., 2018), since a short lifetime reflects high conjugation between fluorophores and vice-versa. Lifetime fluorescence variation could be visualized in the corresponding lifetime color-coded images of the poplar cell walls (Fig. 3I-L), from green to yellow, meaning that lifetime was decreased with increased DAP severity. At the cell wall level, fluorescence lifetime in SW appeared always slightly longer than in CML and

CC for all poplar samples considered (Fig. 4M-P). This can be explained by the differences in the chemical structure of lignin and its molecular environment in these regions, suggesting that both CC and CML regions contain short lifetime component (condensed lignin: *p*-hydroxyphenyl units) and SW regions contain both short and long lifetime components (loosely packed lignin) (Donaldson & Radotic, 2013; Zeng et al., 2015). Untreated poplar fluorescence lifetime was about 813 ± 25.22 ps, then increased significantly to 885 ± 29.17 ps for severity of 2.4; p-value < 0.05 (p-value = 0.045) and even reached 966 ± 34.87 ps for severity of 2.5 (p-value = 0.01), suggesting DAP increased the content of loosely-packed lignin by depolymerising dense lignin regions (Li et al., 2007). In contrast, DAP with the highest severity of 2.7 led to a drop of poplar fluorescence lifetime by 40% to 585 ± 30.49 ps (p-value <0.001), suggesting the existence of a threshold effect around CSF 2.5-2.7. Indeed, it seems the population of denser lignin has suddenly extended in all considered cell wall regions because of the extraction of the loosely packed lignin during the solubilisation of hemicellulose and the formation of pseudo-lignin. Such harsh conditions have probably generated lignin degradation products which have been able to repolymerize as highly conjugated polymers with shortened fluorescence lifetime (Sannigrahi et al., 2011; Trajano et al., 2013).

Overall, fluorescence analysis reveals that DAP strongly alters lignin itself and its environment mainly due to partial lignin depolymerization and hemicellulose solubilisation on the range of CSF 2.4-2.5, while higher CSF of 2.7 generates lignin chemical modifications such as lignin condensation and creation of new inter-linkages between fluorophores.

3.5 DAP induces significant shape changes at cellular scale

Images obtained using scanning electron microscopy indicated structural changes at cellular scale on pretreated samples compared to untreated samples. However, the drawbacks of SEM imaging including artifacts potentially introduced by sample preparation (drying) and limited spatial dimensions (2D) have led to a mostly qualitative conclusions so far (Herbaut et al., 2018; Chen et al., 2018). To quantitatively investigate the effect of pretreatment at cellular scale and study its correlation with acquired spectral and chemical data, an original method combining 3D confocal acquisition and 3D segmentation and quantification was developed (see Materials and Methods) and the morphological parameters including cell volumes, surface areas and subsequently cellular sphericity, a dimensionless cellular scale structural parameter, were computed. The mean sphericity values were 0.62 ± 0.19, 0.54 ± 0.21, 0.52 ± 0.19, 0.43 ± 0.11 for untreated, and pretreated samples at 2.4 CSF, 2.5 CSF, 2.7 CSF respectively. The quantifications showed that cellular sphericity gradually decreased as the DAP pretreatment severity increased (Kruskal–Wallis test, *p*-value = 7e-109,) (Fig. 4), with the most striking cell shape alteration at 2.7 CSF. The decreasing trend in cell sphericity with increasing pretreatment severity confirms the morphological changes observed in SEM images and can be explained by the fact that the pretreatment modifies the compact structure of cell walls through dissolution of hemicelluloses and solubilisation and redistribution of lignin therefore decreases cell compactness measured by sphericity. Moreover, sphericity as a function of the computed cell volume over computed surface area, decreases by increasing surface area which has been previously reported (Torr et al., 2016; Zhang et al., 2018). Our results show that measurements of cell sphericity can provide quantitative useful information about the DAP severity and consequently predict hydrolysis yield. The results also highlight the importance of multi-scale approaches involving cellular and tissular

scale in thoroughly investigating LB recalcitrance and shed light on parameters behind LB recalcitrance at scales yet little explored.

3.6 Correlation analysis of measured chemical, spectral and structural parameters reveals quantitative relationships across scales

Given the different properties determined for the untreated and DAP poplar samples, results clearly show strong correlations between DAP severity and modifications in chemical composition (in particular lignin) together with structural modifications, in different cell wall regions. Importantly, a threshold effect has been identified as severity was increased from CSF 2.5 to 2.7, revealing that an increase of only 5 minutes of DAP has dramatic consequences on polymer organization as revealed by spectral analysis. Consequently, these data can be useful to understand the correlation between related factors and saccharification potential. Indeed, lignocellulose chemical and structural complexity limit the establishment of easy and low-cost transformation processes, and many studies have searched to find some factors that could help predicting recalcitrance (Auxenfans et al., 2017b; Chabbert et al., 2018; Huang et al., 2017; Paës et al., 2019). To understand relationships between parameters, we conducted a detailed correlation analysis between quantified parameters from **autofluorescence, FLIM, Raman and structural analysis and hydrolysis yield at 72 hrs (Fig. 5).**

Among spectral factors, fluorescence lifetime appears as a strong predictor of hydrolysis (correlation values ca. 0.70-0.75), while autofluorescence and Raman data showed much stronger correlations (0.95-1) and can thus be considered as excellent predictors of hydrolysis. Regarding autofluorescence, its capacity to predict hydrolysis was previously demonstrated on different biomass species and different pretreatment types (Herbaut et al., 2018; Auxenfans et al., 2017a), which strengthens its potential universality. This means

449 that autofluorescence, more than fluorescence lifetime, reveals accessibility of enzymes to
450 polysaccharides, probably because it is related to both structure and composition of lignin.
451 Nonetheless, lifetime analysis is also relevant to understand the chemical modifications of
452 lignin during pretreatment. Raman data are also a good compromise to predict hydrolysis
453 by using specific ratio between lignin and cellulose-related bands, which is directly related
454 to polymer accessibility.
455 Furthermore, cellular scale morphological parameter, namely sphericity is identified which
456 exhibits a strong negative correlation with hydrolysis yield (-0.96, p-value < 0.05). This
457 demonstrates that a structural factor can be measured at cellular scale correlated with DAP
458 severity can predict saccharification. Even though, it was previously demonstrated that
459 nanoscale structural features (porosity, cellulose accessible surface for example) were
460 related to hydrolysis (Herbaut et al., 2018; Zhang et al., 2018; Kruyeniski et al., 2019), it is
461 the first time to our knowledge that a cellular scale feature like sphericity can also predict
462 hydrolysis. This reveals some un-commonly studied connections between scales:
463 hydrolysis by enzymes occurs at the nano-scale, but cell shape might be a strong marker of
464 polymer organization.

465 **4. Conclusions**

466 Multiscale analysis of dilute-acid pretreated poplar samples revealed that several markers
467 could help understanding the effect of pretreatment on polymer composition and
468 organization and subsequently hydrolysis. In particular, autofluorescence appears as a
469 marker previously identified, thus likely to be considered as pivotal. Importantly, the
470 results show that cellular scale structural parameters such as cellular sphericity, seem also
471 to be strongly correlated with hydrolysis which should be further studied using other

472 biomass species and pretreatments, including investigating other structural markers to
473 assay their universality.
474
475 **Acknowledgements**
476 Valérie Untereiner is acknowledged for her help in performing Raman measurement,
477 Anouck Habrant for her relevant guidance in confocal measurement, François Gaudard for
478 his help in performing the SEM observations and Mickaël Frye for FLIM measurements.
479 This work is supported by Grand Est Region and FEDER (PhD TECMI-4D scholarship
480 project to A.Z.), and INRA ANS Grant LIMO4DE (to Y.R.).
481
482 **References**
483 1. Trends, G. 2017. Challenges and Opportunities in the Implementation of the Sustainable
484 Development Goals.
485 2. Yuan, Z., Wen, Y., Li, G. 2018. Production of bioethanol and value added compounds
486 from wheat straw through combined alkaline/alkaline-peroxide pretreatment.
487 Bioresour. Technol. 259, 228-236.
488 3. Zhao, X., Zhang, L., Liu, D. 2012a. Biomass recalcitrance. Part II: Fundamentals of
489 different pre-treatments to increase the enzymatic digestibility of lignocellulose.
490 Biofuel. Bioprod. Biorefin. 6, 561-579.
491 4. Zhao, X., Zhang, L., Dehua Liu. 2012b. Biomass recalcitrance. Part I: the chemical
492 compositions and physical structures affecting the enzymatic hydrolysis of
493 lignocellulose. Biofuel. Bioprod. Biorefin. 6, 465-482.
494 5. Studer, M.H., DeMartini, J.D., Davis, M.F., Sykes, R.W., Davison, B., Keller, M.,
495 Tuskan, G.A., Wyman, C.E. 2011. Lignin content in natural Populus variants
496 affects sugar release. Proceedings of the National Academy of Sciences. 108, 6300-
497 6305.
498 6. Xu, H., Che, X., Ding, Y., Kong, Y., Li, B., Tian, W. 2019. Effect of crystallinity on
499 pretreatment and enzymatic hydrolysis of lignocellulosic biomass based on
500 multivariate analysis. Bioresour. Technol. 279, 271-280.
501 7. Hallac, B.B., Ragauskas, A.J. 2011. Analyzing cellulose degree of polymerization and
502 its relevancy to cellulosic ethanol. Biofuel. Bioprod. Biorefin. 5, 215-225.
503 8. Meng, X., Wells, T., Sun, Q., Huang, F., Ragauskas, A. 2015. Insights into the effect of
504 dilute acid, hot water or alkaline pretreatment on the cellulose accessible surface
505 area and the overall porosity of Populus. Green Chemistry. 17, 4239-4246.
506 9. McCann, M.C., Carpita, N.C. 2015. Biomass recalcitrance: a multi-scale, multi-factor,
507 and conversion-specific property. Journal of experimental botany. 66, 4109-4118.
508 10. Silveira, M.H.L., Morais, A.R.C., da Costa Lopes, A.M., Olekszyszen, D.N., Bogel-
509 Łukasik, R., Andreaus, J., Pereira Ramos, L. 2015. Current pretreatment

technologies for the development of cellulosic ethanol and biorefineries. ChemSusChem. 8, 3366-3390.
11. Cao, S., Pu, Y., Studer, M., Wyman, C., Ragauskas, A.J. 2012. Chemical transformations of Populus trichocarpa during dilute acid pretreatment. RSC Advances. 2, 10925.
12. Santos, V.T.d.O., Siqueira, G., Milagres, A.M.F., Ferraz, A. 2018. Role of hemicellulose removal during dilute acid pretreatment on the cellulose accessibility and enzymatic hydrolysis of compositionally diverse sugarcane hybrids. Ind Crops Prod. 111, 722-730.
13. Lee, J.-W., Jeffries, T.W. 2011. Efficiencies of acid catalysts in the hydrolysis of lignocellulosic biomass over a range of combined severity factors. Bioresour. Technol. 102, 5884-5890.
14. Chang, C., Bowman, J.L., Meyerowitz, E.M. 2016. Field guide to plant model systems. Cell. 167, 325-339.
15. Meng, X., Pu, Y., Yoo, C.G., Li, M., Bali, G., Park, D.Y., Gjersing, E., Davis, M.F., Muchero, W., Tuskan, G.A. 2017. An In-Depth Understanding of Biomass Recalcitrance Using Natural Poplar Variants as the Feedstock. ChemSusChem. 10, 139-150.
16. Chum, H.L., Johnson, D.K., Black, S.K. 1990. Organosolv pretreatment for enzymic hydrolysis of poplars. 2. Catalyst effects and the combined severity parameter. Industrial & engineering chemistry research. 29, 156-162.
17. Herbaut, M., Zoghlami, A., Habrant, A., Falourd, X., Foucat, L., Chabbert, B., Paes, G. 2018. Multimodal analysis of pretreated biomass species highlights generic markers of lignocellulose recalcitrance. Biotechnol. Biofuels. 11, 52.
18. Auxenfans, T., Cronier, D., Chabbert, B., Paes, G. 2017a. Understanding the structural and chemical changes of plant biomass following steam explosion pretreatment. Biotechnol. Biofuels. 10, 36.
19. Zeng, Y., Yarbrough, J.M., Mittal, A., Tucker, M.P., Vinzant, T.B., Decker, S.R., Himmel, M.E. 2016. In situ label-free imaging of hemicellulose in plant cell walls using stimulated Raman scattering microscopy. Biotechnol Biofuels. 9, 256.
20. Gierlinger, N., Keplinger, T., Harrington, M. 2012. Imaging of plant cell walls by confocal Raman microscopy. Nature Protocl. 7, 1694-708.
21. Chen, S., Zhang, X., Ling, Z., Ji, Z., Ramarao, B.V., Ramaswamy, S., Xu, F. 2016a. Probing and visualizing the heterogeneity of fiber cell wall deconstruction in sugar maple (Acer saccharum) during liquid hot water pretreatment. RSC Advances. 6, 79297-79306.
22. Willis, L., Refahi, Y., Wightman, R., Landrein, B., Teles, J., Huang, K.C., Meyerowitz, E.M., Jönsson, H. 2016. Cell size and growth regulation in the Arabidopsis thaliana apical stem cell niche. Proceedings of the National Academy of Sciences. 113, E8238-E8246.
23. Michelin, G., Refahi, Y., Wightman, R., Jönsson, H., Traas, J., Godin, C., Malandain, G. 2016. Spatio-temporal registration of 3D microscopy image sequences of Arabidopsis floral meristems. *2016 IEEE 13th International Symposium on Biomedical Imaging (ISBI)*. IEEE. pp. 1127-1130.
24. Schroeder, W.J., Lorensen, B., Martin, K. 2004. *The visualization toolkit: an object-oriented approach to 3D graphics*. Kitware.
25. Esteghlalian, A., Hashimoto, A.G., Fenske, J.J., Penner, M.H. 1997. Modeling and optimization of the dilute-sulfuric-acid pretreatment of corn stover, poplar and switchgrass. Bioresour. Technol. 59, 129-136.

559 26. Sannigrahi, P., Kim, D.H., Jung, S., Ragauskas, A. 2011. Pseudo-lignin and
560 pretreatment chemistry. Energy. Environ. Sci. 4, 1306-1310.
561 27. Chen, L., Li, J., Lu, M., Guo, X., Zhang, H., Han, L. 2016b. Integrated chemical and
562 multi-scale structural analyses for the processes of acid pretreatment and enzymatic
563 hydrolysis of corn stover. Carbohydrate polymers. 141, 1-9.
564 28. An, S., Li, W., Liu, Q., Xia, Y., Zhang, T., Huang, F., Lin, Q., Chen, L. 2019.
565 Combined dilute hydrochloric acid and alkaline wet oxidation pretreatment to
566 improve sugar recovery of corn stover. Bioresour. Technol. 271, 283-288.
567 29. Meng, X., Sun, Q., Kosa, M., Huang, F., Pu, Y., Ragauskas, A.J. 2016.
568 Physicochemical Structural Changes of Poplar and Switchgrass during Biomass
569 Pretreatment and Enzymatic Hydrolysis. ACS Sustainable Chemistry &
570 Engineering. 4, 4563-4572.
571 30. Linde, M., Jakobsson, E., Galbe, M., Zacchi, G. 2008. Steam pretreatment of dilute
572 H2SO4-impregnated wheat straw and SSF with low yeast and enzyme loadings for
573 bioethanol production. Biomass. Bioenergy. 32, 326-332.
574 31. Chen, S., Ling, Z., Zhang, X., Kim, Y.S., Xu, F. 2018. Towards a multi-scale
575 understanding of dilute hydrochloric acid and mild 1-ethyl-3-methylimidazolium
576 acetate pretreatment for improving enzymatic hydrolysis of poplar wood. Ind Crops
577 Prod. 114, 123-131.
578 32. Negro, M., Manzanares, P., Oliva, J., Ballesteros, I., Ballesteros, M. 2003. Changes in
579 various physical/chemical parameters of Pinus pinaster wood after steam explosion
580 pretreatment. Biomass. Bioenergy. 25, 301-308.
581 33. Mansfield, S.D., Mooney, C., Saddler, J.N. 1999. Substrate and enzyme characteristics
582 that limit cellulose hydrolysis. Biotechnol. Prog. 15, 804-816.
583 34. Ling, Z., Ji, Z., Ding, D., Cao, J., Xu, F. 2015. Microstructural and topochemical
584 characterization of thermally modified poplar (*Populus cathayaha*) cell wall.
585 BioResources. 11, 786-799.
586 35. Gierlinger, N., Schwanninger, M. 2006. Chemical imaging of poplar wood cell walls
587 by confocal Raman microscopy. Plant physiology. 140, 1246-54.
588 36. Ma, J., Zhou, X., Zhang, X., Xu, F. 2013. Label-free in situ Raman analysis of opposite
589 and tension wood in Populus nigra. BioResources. 8, 2222-2233.
590 37. Ji, Z., Ling, Z., Zhang, X., Yang, G.-H., Xu, F. 2014. Impact of alkali pretreatment on
591 the chemical component distribution and ultrastructure of poplar cell walls.
592 BioResources. 9, 4159-4172.
593 38. Donaldson, L., Radotic, K. 2013. Fluorescence lifetime imaging of lignin
594 autofluorescence in normal and compression wood. Journal of microscopy. 251,
595 178-187.
596 39. Auxenfans, T., Terryn, C., Paes, G. 2017b. Seeing biomass recalcitrance through
597 fluorescence. Scientific reports. 7, 8838.
598 40. Coletta, V.C., Rezende, C.A., da Conceição, F.R., Polikarpov, I., Guimarães, F.E.G.
599 2013. Mapping the lignin distribution in pretreated sugarcane bagasse by confocal
600 and fluorescence lifetime imaging microscopy. Biotechnol. Biofuels. 6, 43.
601 41. Li, J., Henriksson, G., Gellerstedt, G. 2007. Lignin depolymerization/repolymerization
602 and its critical role for delignification of aspen wood by steam explosion.
603 Bioresour. Technol. 98, 3061-3068.
604 42. Van Munster, E.B., Gadella, T.W. 2005. Fluorescence lifetime imaging microscopy
605 (FLIM). in: *Microscopy techniques*, Springer, pp. 143-175.
606 43. Chabbert, B., Terryn, C., Herbaut, M., Vaidya, A., Habrant, A., Paës, G., Donaldson,
607 L. 2018. Fluorescence techniques can reveal cell wall organization and predict
608 saccharification in pretreated wood biomass. Ind Crops Prod. 123, 84-92.

609 44. Zeng, Y., Zhao, S., Wei, H., Tucker, M.P., Himmel, M.E., Mosier, N.S., Meilan, R.,
610 Ding, S.Y. 2015. In situ micro-spectroscopic investigation of lignin in poplar cell
611 walls pretreated by maleic acid. Biotechnol Biofuels. 8, 126.
612 45. Trajano, H.L., Engle, N.L., Foston, M., Ragauskas, A.J., Tschaplinski, T.J., Wyman,
613 C.E. 2013. The fate of lignin during hydrothermal pretreatment. Biotechnol.
614 Biofuels. 6, 110.
615 46. Torr, K.M., Love, K.T., Simmons, B.A., Hill, S.J. 2016. Structural features affecting
616 the enzymatic digestibility of pine wood pretreated with ionic liquids.
617 Biotechnology and bioengineering. 113, 540-549.
618 47. Zhang, H., Li, J., Huang, G., Yang, Z., Han, L. 2018. Understanding the synergistic
619 effect and the main factors influencing the enzymatic hydrolyzability of corn stover
620 at low enzyme loading by hydrothermal and/or ultrafine grinding pretreatment.
621 Bioresource technology. 264, 327-334.
622 48. Huang, J., Li, Y., Wang, Y., Chen, Y., Liu, M., Wang, Y., Zhang, R., Zhou, S., Li, J.,
623 Tu, Y. 2017. A precise and consistent assay for major wall polymer features that
624 distinctively determine biomass saccharification in transgenic rice by near-infrared
625 spectroscopy. Biotechnol. Biofuels. 10, 294.
626 49. Paës, G., Navarro, D., Benoit, Y., Blanquet, S., Chabbert, B., Chaussepied, B.,
627 Coutinho, P.M., Durand, S., Grigoriev, I.V., Haon, M. 2019. Tracking of enzymatic
628 biomass deconstruction by fungal secretomes highlights markers of lignocellulose
629 recalcitrance. Biotechnol. Biofuels. 12, 76.
630 50. Kruyeniski, J., Ferreira, P.J., Carvalho, M.d.G.V.S., Vallejos, M.E., Felissia, F.E.,
631 Area, M.C. 2019. Physical and chemical characteristics of pretreated slash pine
632 sawdust influence its enzymatic hydrolysis. Ind Crops Prod. 130, 528-536.
633

Figures

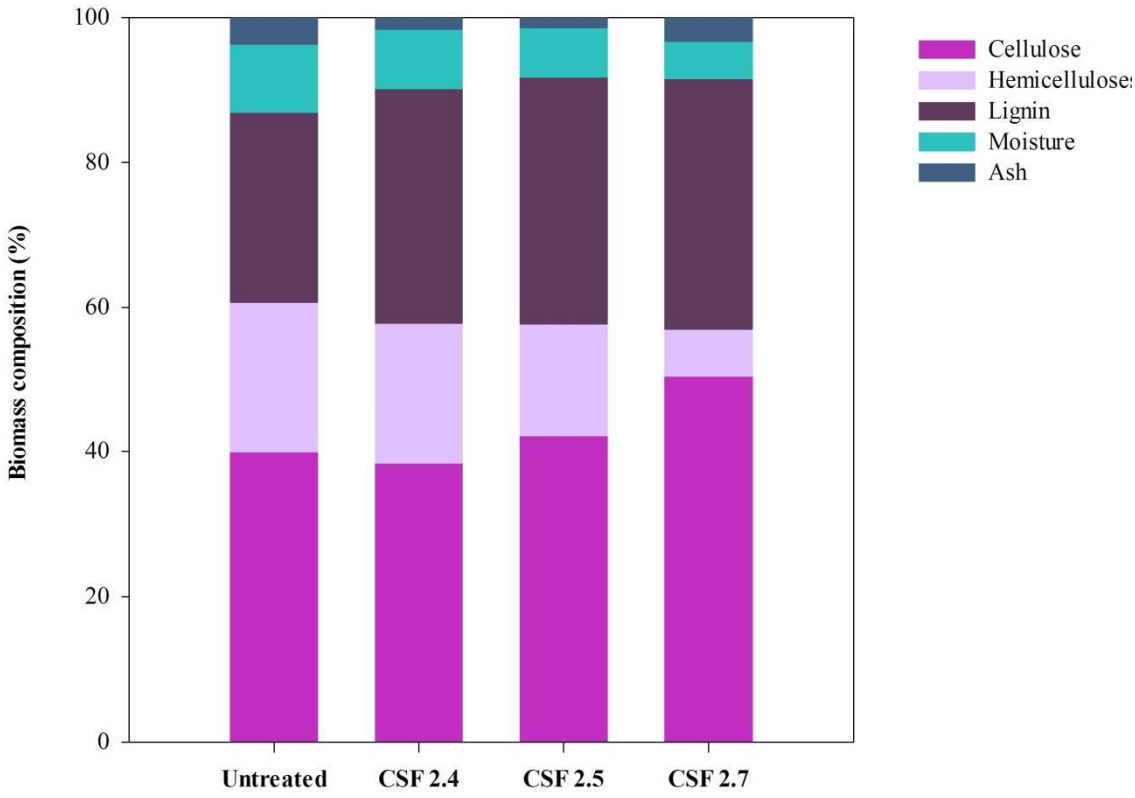

Fig. 1. Chemical composition of untreated and pretreated poplar samples. Contents are expressed as weight percentages (%w/w) of the dry biomass amount.

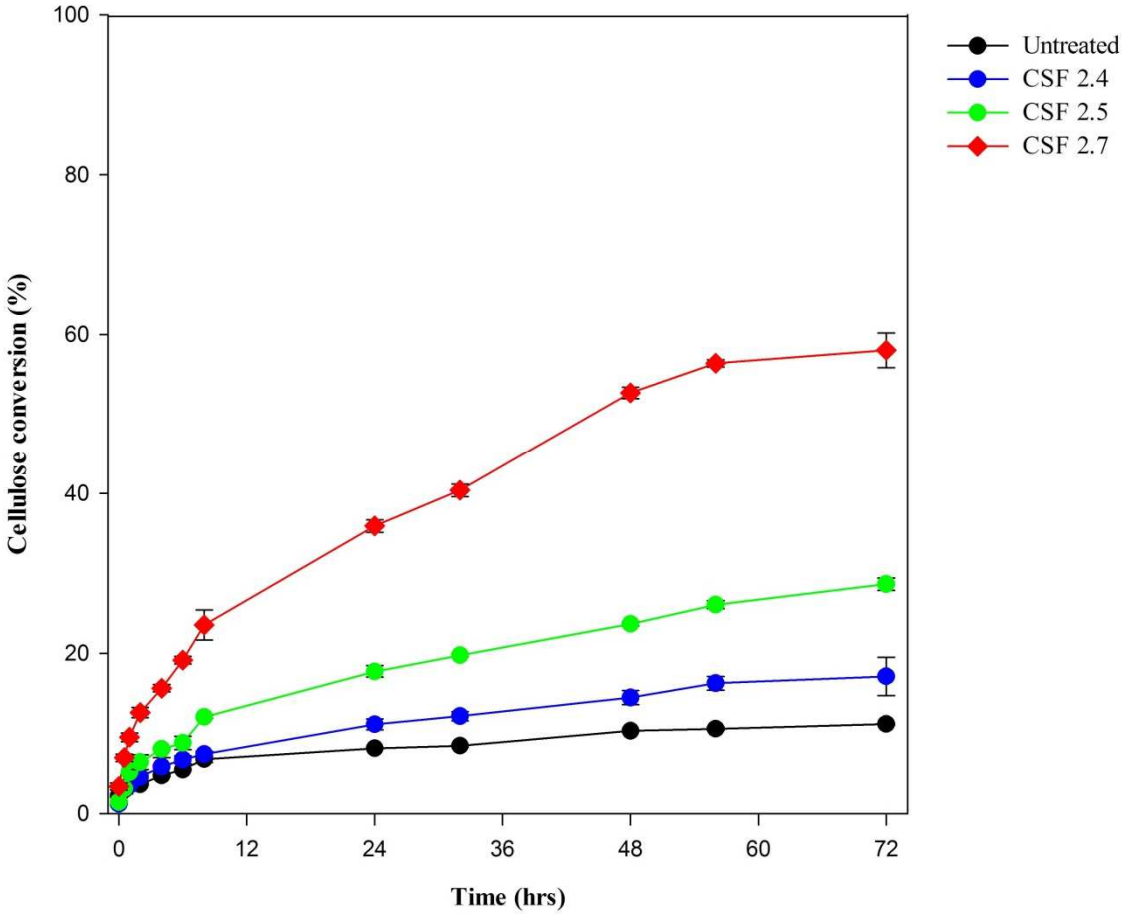

Fig. 2. Cellulose conversion during enzymatic hydrolysis over 72 hrs.

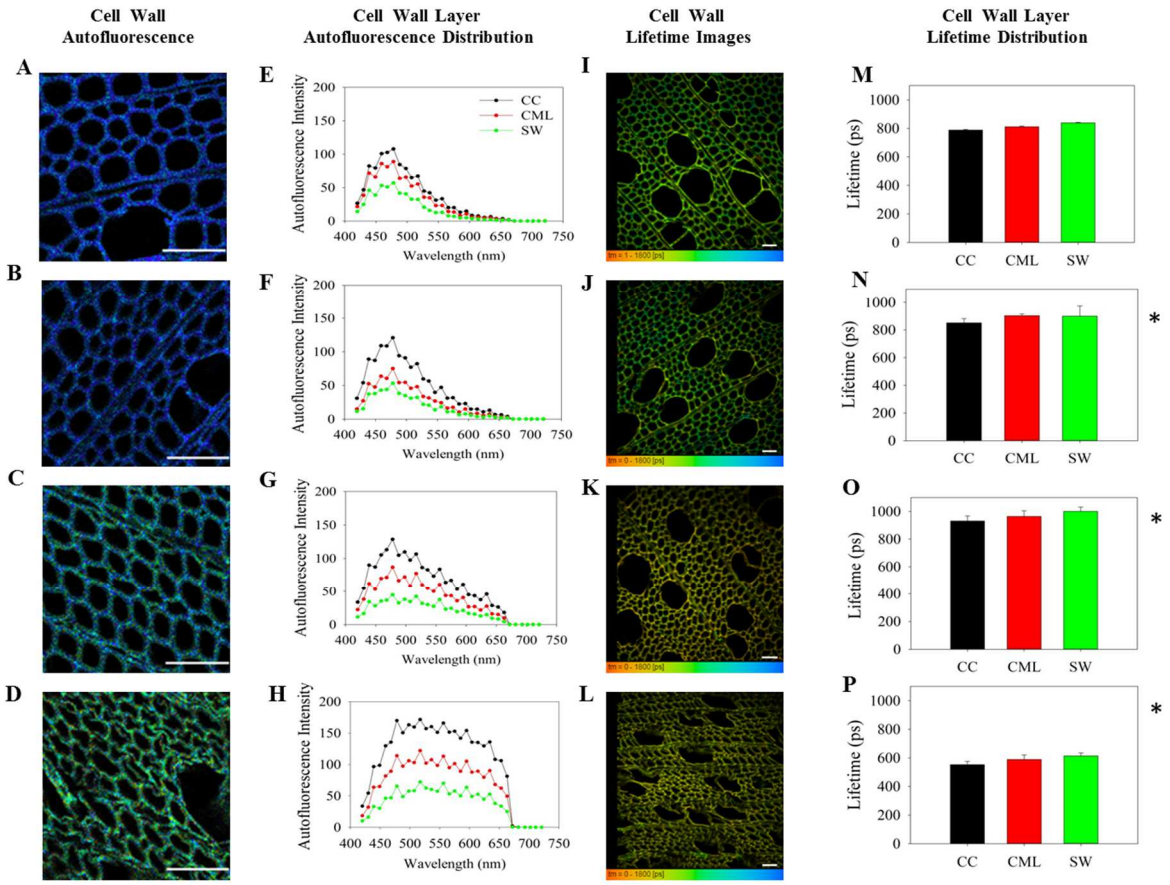

Fig. 3. Fluorescence properties of untreated and pretreated poplar. (A, B, C and D) spectral confocal images of the cell wall cell corner (CC) in black, compound middle lamella (CML) in red, and secondary wall (SW) in green for untreated and pretreated poplar samples illustrating the autofluorescence of lignin generated by 750 nm bi-photon excitation, emission measured from 420 nm (blue) to 722 nm (red), scale bars 20µm. (E, F, G and H) Fluorescence spectra of the cell wall for untreated and pretreated poplar samples. (I, J, K and L) Fluorescence lifetime images and (M, N, O and P) lifetime measurements for untreated and pretreated poplar samples, scale bars 20µm. Fluorescence lifetime values are averaged from measurement on three different samples and three different areas from the same sample. Error bars indicate standard deviation. Asterisks indicate statistically significant difference between pretreated and untreated poplar samples.

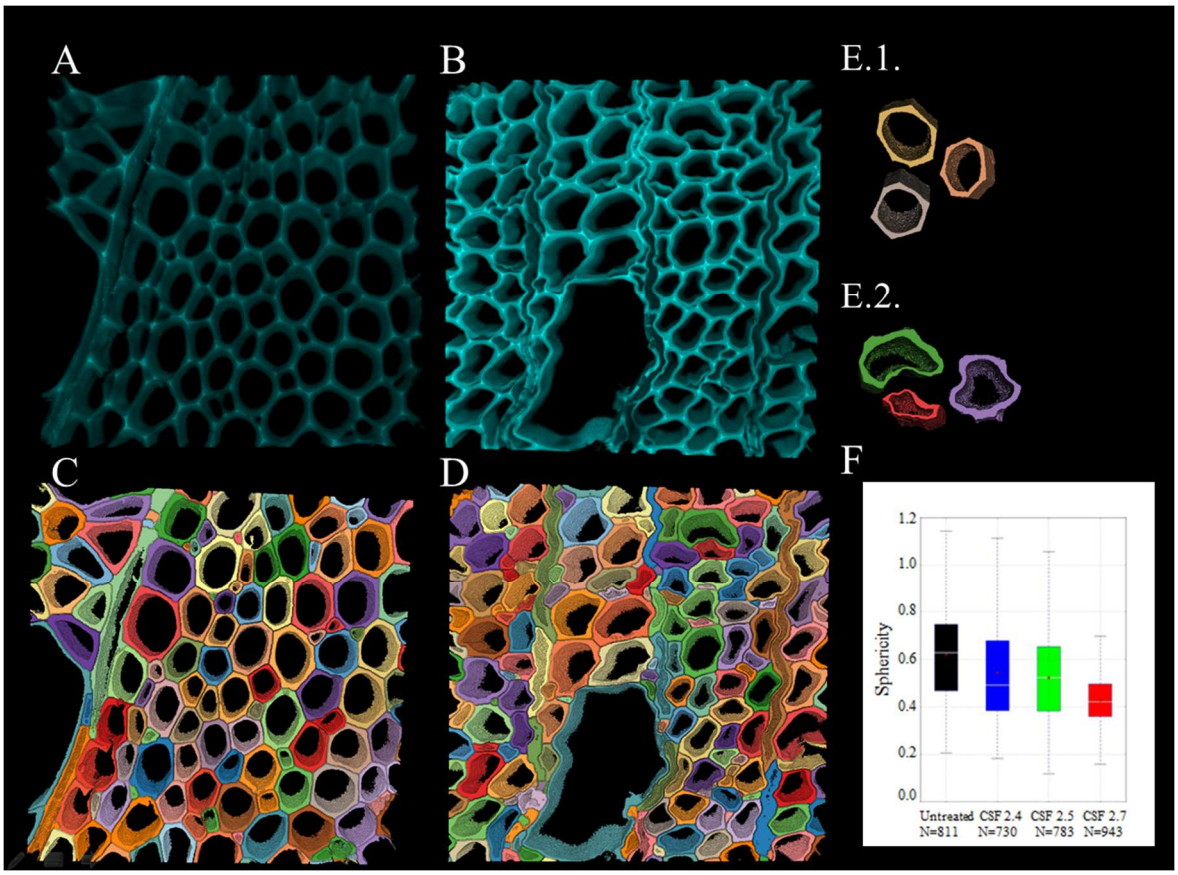

Fig. 4. Effect of DAP on poplar samples at cellular scale. (A) 3D projection of confocal image of untreated poplar section. (B) 3D projection of confocal image of pretreated poplar section at CSF 2.7. (C) Rendering of 3D segmentation of the untreated sample confocal stacks. (D) Rendering of 3D segmentation of the pretreated sample confocal stack. (E.1.) Randomly selected cells showing effect of the segmented untreated sample and (E.2.) and the pretreated sample, showing effect of DAP on individual cell shapes. (F) Distribution of cellular sphericity of untreated and pretreated samples with different severity conditions. The boxes represent the interquartile range and the white lines in the boxes represent the medians. The whiskers show the range of values from the highest to the lowest excluding outliers (not shown). N is the number of segmented cells.

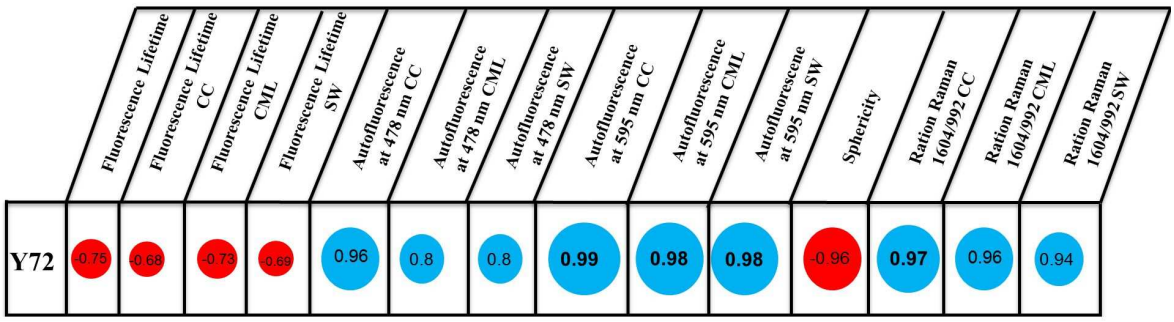

Fig. 5 Pearson's correlation coefficients between quantified spectral, structural factors and hydrolysis yield (p-value <0.05).

Tables

Table 1. Raman bands and their assignment to lignin and carbohydrate components (cellulose, glucomannan and xylan) according to the literature. str: stretching

Wavenumbers (cm^{-1})	Components	Assignments
992	Cellulose	Heavy atom (CC and CO) str.
1036	Cellulose	HCC and HCO bending
1095	Cellulose Glucomannan Xylan	Heavy atom (CC and CO) str.
1123	Cellulose Glucomannan Xylan	Heavy atom (CC and CO) str.
1150	Cellulose	Heavy atom (CC and CO) str. plus HCC and HCO bending
1275	Lignin	Aryl-O of aryl OH and aryl O−CH3; guaiacyl ring (with C=O group)
1331	Lignin	HCC and HCO bending
1376	Cellulose	HCC, HCO, and HOC bending
1604	Lignin	aryl ring str., sym.
1660	Lignin-CAA	ring conjugated C=C str. of coniferyl alcohol; C=O str. of coniferaldehyde

Graphical abstract